

Soil phosphorus crisis in the Tibetan alpine permafrost region

Received: 9 July 2024

Accepted: 24 June 2025

Published online: 05 July 2025



Jiangtao Hong^{1,6}, Bo Pang^{1,2,6}, Lirong Zhao^{1,2}, Shumiao Shu^{1,3}, Puyu Feng^{1,4}, Fang Liu^{1,2}, Ziyin Du⁵ & Xiaodan Wang¹✉

Phosphorus (P) is an essential nutrient for living systems and is critical to the functioning of ecosystems. Permafrost areas have a huge reservoir of soil P that is currently not used very much; however, the direction and magnitude of changes in soil P stocks across the Tibetan alpine permafrost regions over recent decades remain unclear and the P budget has not been well assessed. Here we use a unique combination of a soil resampling method and a modified process-balanced model to assess the historical dynamics of soil P pools (0–30 cm depth) and the key flows of P in ecosystems across Tibetan alpine permafrost region. Compared with the 1980s, the soil P stock decreases dramatically by 36.1% in the 2020 s, decreasing from 346.5 to 221.4 Tg P (1 Tg = 10^{12} g) during the last three decades. Water erosion accounts for 82.3% of the total soil P outflow. Our projections suggest that the soil P stock will only be 20.3% of the 1980s stock by the end of this century, leading to an unprecedented crisis of P limitation in permafrost regions.

Phosphorus (P) is a key element in organic molecules (e.g., nucleic acids, ATP and phospholipids) and has an important role in regulating the growth, development and reproduction of living organisms^{1–4}. Permafrost regions occupy about 24% of the land surface in the northern hemisphere⁵, but their soil P reserves account for >30% of the northern hemisphere total (soil depth of 0–30 cm, calculated according to ref. 6). Permafrost soils contain a huge reservoir of P as a result of the rejuvenation of soils, weak leaching processes and the low uptake of nutrients by plants, and can therefore be regarded as important reserves of P in terrestrial ecosystems⁶.

The recent rapid changes in the Earth's climate are simultaneously causing the widespread degradation of permafrost⁷ and altering the hydrology of high-latitude/high-altitude regions⁸, exposing mineral nutrients previously protected in permafrost to transport and processing in lakes, rivers, and estuaries^{9,10}. The unidirectional flow of P from terrestrial ecosystems to freshwater bodies and, eventually, the oceans is considered to be the greatest sustainability challenge in the P cycle¹¹. The redistribution of P on spatiotemporal scales could regulate the composition

of local, downstream, and even coastal plant communities, as well as the net primary productivity and health of the environment^{12,13}. In addition, the availability of P alters the trajectory of the permafrost carbon (C) cycle by influencing gross primary productivity and net ecosystem productivity^{14,15}, and the associated fluxes of C in aquatic sediments¹² by influencing soil microbial processes and greenhouse gas emissions. This can have a positive or negative feedback role in global climate change. Therefore, quantifying the temporal changes of the P stored in permafrost is crucial and urgently needed in guiding strategies to tackle the grand challenge of future P limitation^{11,16}, as well as the environmental crisis caused by huge losses of P into water bodies that pushes the Earth's environment to its boundary, beyond which come abrupt environmental changes with catastrophic impacts^{17,18}.

Several approaches have been used to explore the historical dynamics of soil P, including soil sample analysis and P budget models^{11,19,20}. The resampling method can accurately estimate historical changes in the soil pool of elements at large spatial scales^{21–23}.

¹Institute of Mountain Hazards and Environment, Chinese Academy of Sciences, Chengdu, China. ²University of Chinese Academy of Sciences, Beijing, China.

³Tuojiang River Basin High-Quality Development Research Center, Neijiang Normal University, Neijiang, China. ⁴College of Land Science and Technology, State Key Laboratory of Efficient Utilization of Agricultural Water Resources, China Agricultural University, Beijing, China. ⁵School of Geographical Sciences, China West Normal University, Nanchong, China. ⁶These authors contributed equally: Jiangtao Hong, Bo Pang. ✉e-mail: wxd@imde.ac.cn

Process-balanced modeling approaches have been used to detect P flows and their drivers in cropland soils over time^{1,2}, demonstrating that water erosion¹¹, absorption by plants¹⁹, food production^{2,20} and/or the recycling of animal manure²⁴ might have a major impact on the soil P balance. Despite advances in our understanding of the P budget over recent decades, substantial uncertainties remain about how much P is lost from soils^{1,11,19,25,26}. The main cause of these discrepancies is that our understanding of current processes and historical soil nutrient availability data are lagging behind the needs of mass balance models²⁷.

As the largest extent of alpine permafrost in the world²⁸, the Tibetan Plateau is an important pool of mineral nutrient elements globally, with 25% of the material flux reaching the ocean coming from this area, despite the fact that it represents only 5% of the Earth's land surface^{6,29}. A few studies have used observations from non-resampling methods to explore the historical changes in total P³⁰ and available P (AP)³¹ in alpine soils. However, the quantity of SPS that have been lost across Tibetan alpine permafrost regions over recent decades remains unclear, and the P

budget of permafrost has not been well assessed. Moreover, substantial uncertainties exist in the projected direction and magnitude of soil P changes, originating from the scarcity of observational broad-scale soil resampling data.

In this study, we used a unique combination of soil resampling and model simulations to assess the temporal changes of soil P pools and the key flows of P in the Tibetan alpine permafrost region (Fig. 1). First, we performed a broad-scale repeat soil survey to obtain data for the soil P density (SPD) in the 1980s and the 2020s. We then built a process-based model of the P flow in ecosystems (MPFE) to simulate changes in the soil P budget from the 1980s to the 2020s according to the mass balance principle. A notable difference between this work and previous studies is that the soil P data were repeatedly measured in situ for the two time periods to verify and improve the accuracy of the MPFE. We predicted the soil P budget up to the year 2100 using the MPFE according to the Shared Socioeconomic Pathway (SSP) SSP1-2.6, SSP2-4.5, SSP3-7.0, and SSP5-8.5 future climate scenarios, providing scientific support for predicting future P balances in permafrost regions.

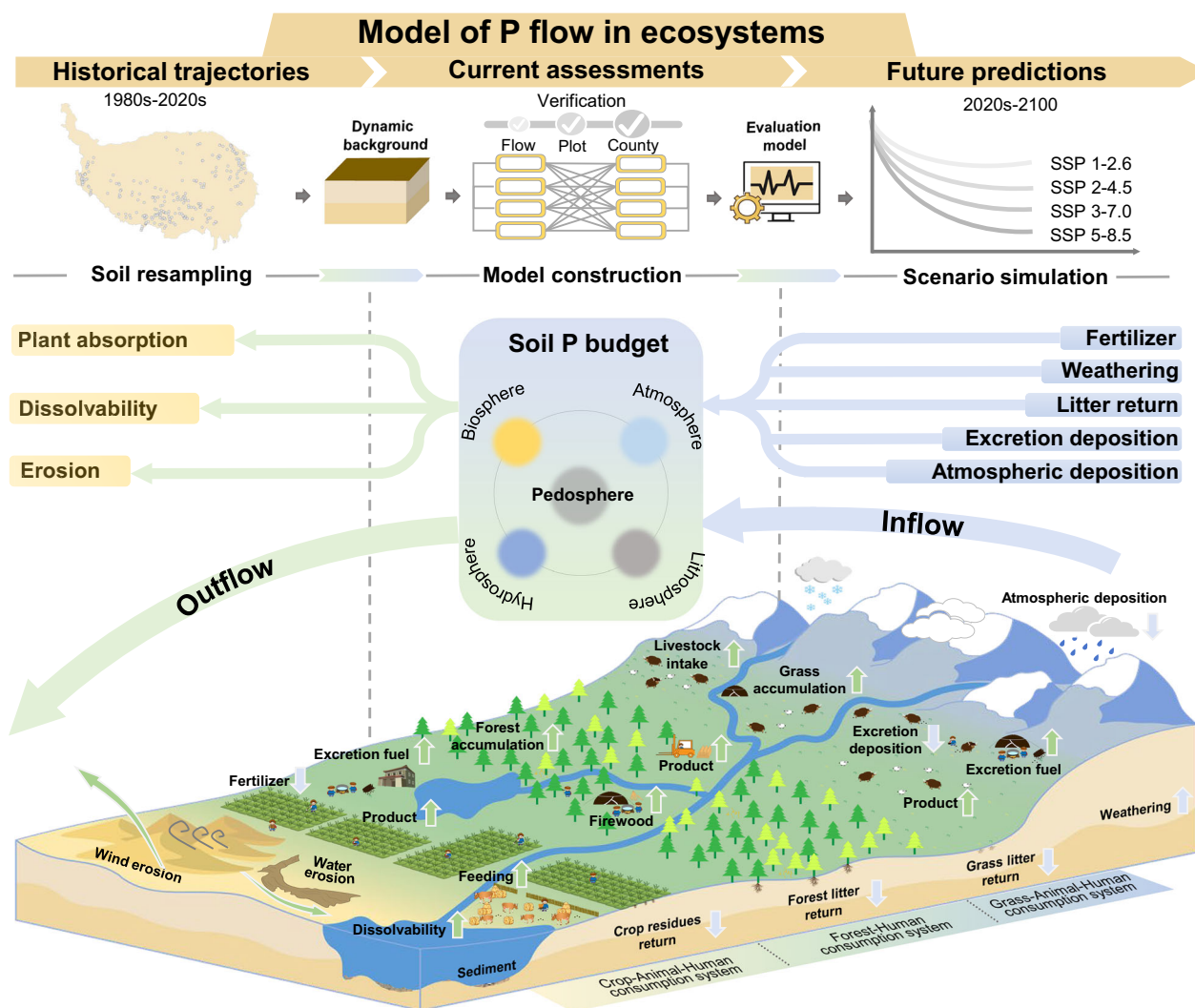


Fig. 1 | Schematic model of P flow in ecosystems (MPFE) in the Tibetan alpine permafrost region. The MPFE includes historical trajectories, current assessments, and future predictions of the soil P budget. The soil resampling P data provided the dynamic background of soil nutrients used to verify and improve the accuracy of the MPFE. The proven MPFE was then used to predict the soil P budget until 2100 according to different scenarios. The MPFE consists of the main key P inflow (weathering, atmospheric deposition, fertilizer, the deposition of livestock

excretions, and the return of plant litter) and outflow (plant absorption, soil erosion, and dissolved P in runoff) subsystems. The net change in the soil P is the P inflow minus the P outflow. The plant-related P flows are defined as *plant-animal-human consumption* systems, consisting of three subsystems: *grass-animal-human consumption* system, *forest-human consumption* system and *crop-animal-human consumption* system. The boundary of the Tibetan Plateau was sourced from Zhang et al.⁹⁴.

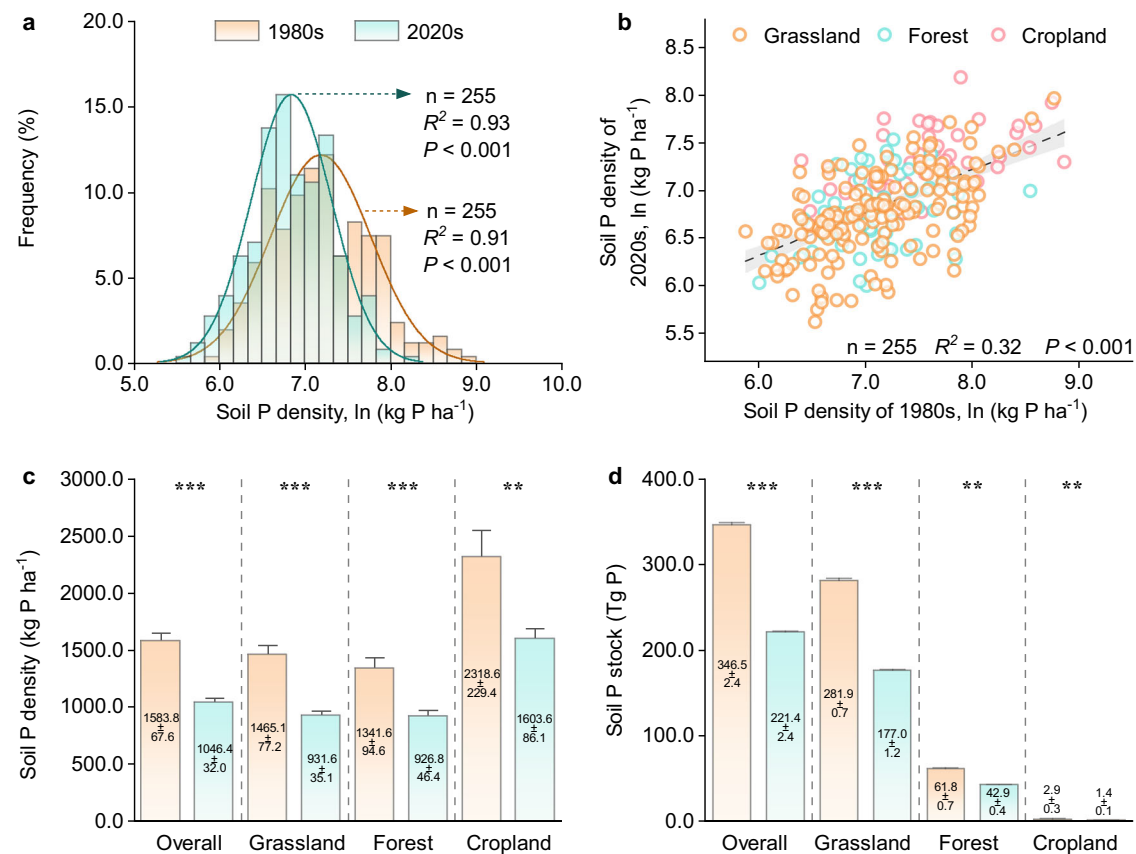


Fig. 2 | Changes in soil P density and stock from the 1980s to the 2020s based on resampling observations. **a** Frequency distributions of the soil P density during the two sampling periods. The soil P density is fitted with a ln-normal distribution and the horizontal axis is displayed on a ln scale. The frequencies of samples are shown as bars, with the curves for the probability density functions shown as orange (1980s) and blue (2020s) lines. **b** Relationships between soil P density in the 1980s and the 2020s. The soil P density is fitted with a ln-normal distribution. The dashed line indicates the ordinary least-squares fit of the linear equation for soil P density between the two sampling periods. The shading accompanying the dashed

fitted line represents the 95% confidence interval. **c** Changes in the soil P density during the two sampling periods. The temporal changes of the soil P density were examined with linear mixed-effects models in which the fixed effect was the sampling period and the random effect was the sampling plot. Asterisks indicate that the null hypothesis could be rejected at a significance level of **0.01 and ***0.001. The standard errors are indicated in part **c**. The error bars represent 95% confidence intervals. **d** Changes in the soil P stock derived from the large-scale resampling investigations. The change in soil P stock was calculated based on the P density and the proportion of each soil type in a given ecosystem.

Results and discussion

Rapid decreases in soil P since the 1980s

We built a unique dataset composed of two parts separated by three decades of time to evaluate the spatiotemporal changes in the density and stock of P in topsoil (0–30 cm depth) across the alpine permafrost regions of the Tibetan Plateau (Supplementary Figs. 1, 2, Supplementary Method 1 and Supplementary Table 1). There was a significant positive correlation between the SPD in the 1980s and 2020s ($R^2 = 0.32$, $P < 0.001$), indicating that the spatial pattern of the SPD had not changed significantly in the past three decades (Fig. 2a, b). However, the SPD showed a significant decrease across the alpine permafrost regions from the 1980s to the 2020s, with the mean SPD decreasing from 1583.8 (± 67.6 SE) to 1046.4 (± 32.0 SE) kg P ha⁻¹ ($P < 0.001$) (Fig. 2c). Further analyses revealed that the SPD tended to decrease among 190 of the total 255 resampling plots and the decline in SPD remained significant until >240 resampling plots were removed from the initial analysis with 255 resampling plots (Supplementary Figs. 3 and 4), demonstrating the robustness of SPD dynamics observed in this study. This decreasing pattern held true in alpine grassland, forest and cropland ecosystems ($P < 0.01$), with the net loss of SPD estimated to be 533.5 kg P ha⁻¹, 414.8 kg P ha⁻¹, and 715.0 kg P ha⁻¹, respectively (Fig. 2c, Supplementary Figs. 3 and 4). The rapid decrease in soil P (14.9 kg ha⁻¹ yr⁻¹) across the Tibetan Plateau was

within the range of the global soil P depletion rate (4–19 kg ha⁻¹ yr⁻¹)¹¹. In terms of the spatial pattern of historical changes in the SPD, the largest decreases in SPD occurred in the central and northeastern Tibetan Plateau, whereas the smallest decrease in SPD was in the western Tibetan Plateau (Supplementary Fig. 3). This may be related to the spatial differences in the quantity of water-induced P loss (Supplementary Fig. 5).

The SPS of the Tibetan permafrost regions decreased dramatically by 36.1% in the 2020s compared with the 1980s, with a gross regional-scale change in the surface SPS of 125.1 Tg P (1 Tg = 10¹² g) over the last three decades ($P < 0.01$) (Fig. 2d). The average net soil P loss of the three ecosystems was approximately 3.5 Tg P yr⁻¹, which is roughly four-fifths of the annual application of chemical P fertilizer to farmland in China (4.2 Tg P yr⁻¹) and one-fifth of the annual application of chemical P fertilizer globally (16.4 Tg P yr⁻¹) (Supplementary Fig. 6). Such a rapid depletion in SPS over a short period of time has not previously been detected and poses a potential crisis in the limitation of P in terrestrial alpine permafrost ecosystems.

Historically negative budget for soil P

The database of the MPFE model developed to simulate the historical trajectories of the P budget consists of the main key P inflow and outflow subsystems (e.g., weathering, atmospheric deposition,

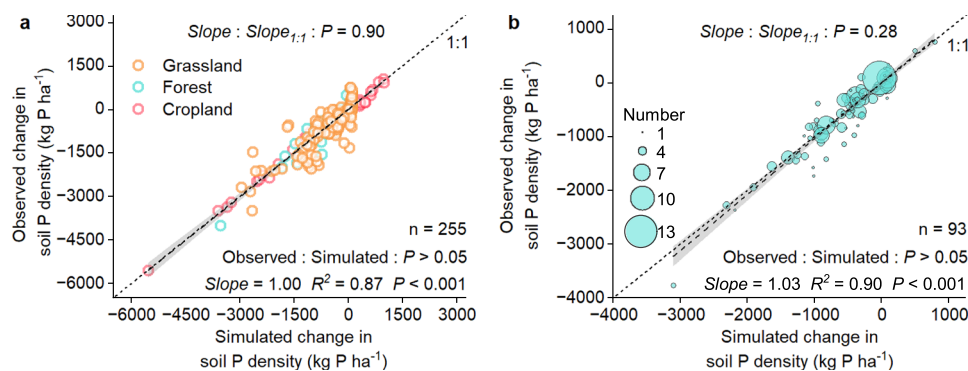


Fig. 3 | Change in soil P density between observations and simulations from the 1980s to the 2020s. a Sampling plots. **b** Counties. Changes in grassland, forest, and cropland are given, and each symbol in part (a) corresponds to one resampling plot. The sizes of the circles in part (b) represent the relative weights of the corresponding observations in each county. The effect of measurements on the soil P density was examined with linear mixed-effects models in which the fixed effect

was the method and the random effect was the sampling plot and county. The effect of methods on soil P density was considered significant if $P < 0.05$. The dashed lines indicate the ordinary least-squares fit of the linear equation of changes in soil P density between the observations and simulations. The shading accompanying the dashed fitted line represents the 95% confidence interval.

fertilizer, absorption by plants, the deposition of livestock excretions, the return of plant litter, livestock feed, livestock, forest and grain products, the burning of firewood and soil erosion) (Supplementary Method 2 and Supplementary Table 2). Similar to conventional modeling approaches^{11,19,20}, we compared our calculations of the main P inflow and outflow subsystems with those of other studies. Most of our modeled P flows were well within the range of published P flows (Supplementary Tables 3–5). To further test the accuracy of our model, we compared the observations and simulations of the change in the SPD between final and first years of observations (Fig. 3a, b). We found three important results: (1) there was fairly good agreement between the simulated and observed temporal changes in SPD at the plot scale ($R^2 = 0.87$, $P < 0.001$) and county scale ($R^2 = 0.90$, $P < 0.001$); (2) the results of the slope test indicated that the simulated and observational data either increased or decreased in equal proportions ($P > 0.05$); and (3) the mixed-effects model showed no significant difference between the geometric mean of the observed and modeled SPD ($P > 0.05$). For a few plots, however, the model had difficulty in capturing the observed temporal changes in SPS. This could have been related to the thin soil thickness used to calculate the SPS preventing us from accounting for vertical migration, or for the uptake of P by plant roots³².

The inflow density of P increased slightly from 4.5, 4.4, 4.7 and 16.2 kg P ha⁻¹ yr⁻¹ to 4.8, 4.6, 4.8, and 39.3 kg P ha⁻¹ yr⁻¹ for the overall ecosystem and the grassland, forest and cropland ecosystems, respectively, from the 1980s to the 2020s ($P < 0.001$) (Fig. 4a–d). Weathering made the highest contribution to the soil P inflow (70.4%) under the effects of the freeze–thaw cycle³³ and glacial denudation³⁴ (Supplementary Discussion 1). The P outflow density decreased significantly from 25.6, 26.4, and 20.6 kg P ha⁻¹ yr⁻¹ to 18.9, 19.4, and 15.4 kg P ha⁻¹ yr⁻¹ for the overall ecosystem and the grassland and forest ecosystems, respectively, from the 1980s to the 2020s ($P < 0.01$) (Fig. 4a–c). The P outflow density of the cropland ecosystem increased significantly from the 1980s to the 2020s ($P < 0.01$) (Fig. 4d). However, the soil P outflow far exceeded the soil P inflow, and therefore the total soil P budget in the alpine permafrost region of the Tibetan Plateau was negative during the last three decades.

Over the same time period, the absorption of P by plants and the dissolved P in runoff accounted for only a small proportion of the total P outflow (13.7%) (Fig. 4e–h, Supplementary Figs. 7 and 8). Among the sub-terms of the absorption of P by plants, the mean annual consumption of P by humans was only 0.3, 0.1, 0.3 and 38.6 kg P ha⁻¹ yr⁻¹ for the overall ecosystem and the grassland, forest and cropland ecosystems, respectively, between the 1980s and 2020s

(Supplementary Fig. 9a–d). Since 2006, the implementation of energy substitution projects³⁵ has led to a significant decrease in the consumption of P by burning animal dung and firewood (Supplementary Fig. 9 and Supplementary Discussion 1). The interannual change in dissolved P was not significant due to the spatial heterogeneity of precipitation across the alpine permafrost region of the Tibetan Plateau³⁶, whereas the increased absorption of P by plants was caused by the recent favorable climatic conditions for plant growth²¹ (Supplementary Discussion 1).

Erosion caused the largest outflow of soil P across the Tibetan Plateau (86.3%) (Fig. 4e–h and Supplementary Fig. 10). Our estimates were further verified by other measurements, such as model simulation and isotope tracing methods (Supplementary Table 4), as well as the seven main regional riverine exports of P (Supplementary Table 5). Among them, the outflow of P caused by water erosion (82.3%) was far greater than that caused by wind erosion (4.0%) (Supplementary Fig. 10). Our area-related calculations resulted in an average outflow of P from the alpine permafrost region caused by water erosion of about 16.1 kg P ha⁻¹ yr⁻¹ (Supplementary Fig. 10a), which is slightly higher than that of previous calculations worldwide (Supplementary Table 6). The annual precipitation is concentrated in the summer months, and the complex conditions of differences in elevation, low vegetation coverage, and the weak resistance to erosion all lead to strong water erosion in this alpine permafrost region³⁷.

The recent trend of warming and humidification has led to the degradation of glaciers and permafrost soils. The increased duration of soil thawing and the advance of the start date of soil thawing could intensify the erodibility of alpine soils and hence increase the supply of sediment^{38,39}. Previous research on northern rivers has established marked increases in discharge and the oceanward flux of alkalinity and associated ions across the pan-Arctic region since the early to mid-20th century, which has been attributed to intensification of the hydrological cycle⁴⁰. However, the increase in vegetation coverage caused by the warming and humidification on the Tibetan Plateau may reduce the intensity of erosion. The insignificant historical change in water erosion across the Tibetan Plateau may have arisen from the counteracting effects of rainfall erosivity factor and vegetation factor (Supplementary Fig. 11). Even if the intensity of soil erosion shows marginal historical changes, the outflow of soil P caused by erosion gradually decreases due to the continuous reduction in soil P concentrations. In addition, the widely distributed floating dunes and desertification in the northwest Tibetan Plateau, on the banks of the Yarlung Zangbo River and in the Qaidam Basin, provide abundant

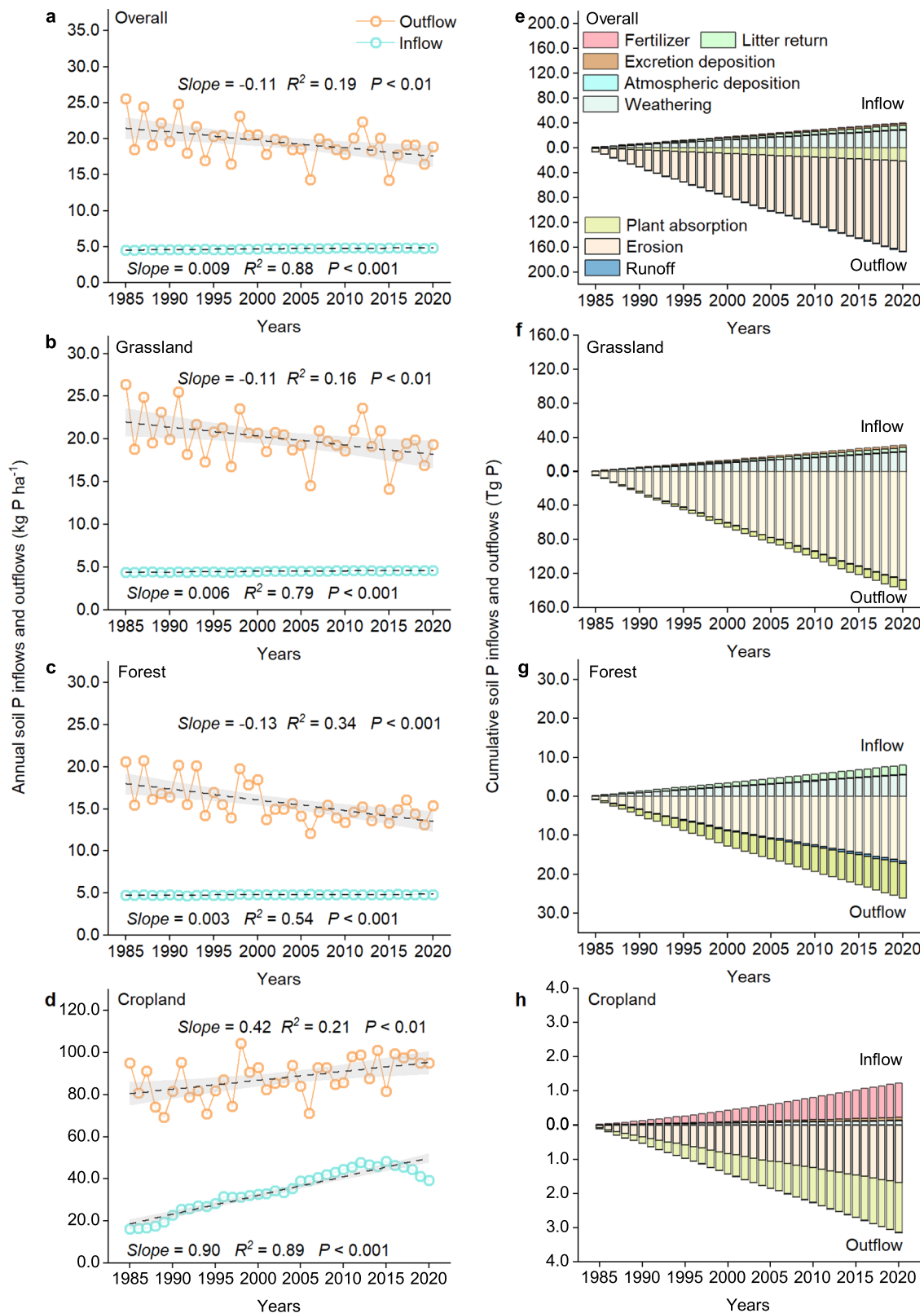


Fig. 4 | Historical trends of annual soil P inflows and outflows in the Tibetan alpine permafrost region for the period from the 1980s to the 2020s. a Annual soil P inflows and outflows for the overall ecosystem. **b** Annual soil P inflows and outflows for grassland. **c** Annual soil P inflows and outflows for forest. **d** Annual soil P inflows and outflows for cropland. **e** Cumulative soil P inflows and outflows for the overall ecosystem. **f** Cumulative soil P inflows and outflows for

grassland. **g** Cumulative soil P inflows and outflows for forest. **h** Cumulative soil P inflows and outflows for cropland. The soil P inflow represents the sum of the supply of P from weathering, atmospheric deposition, fertilizer, the deposition of livestock excretions, and the return of plant litter. The soil P outflow represents the sum of P losses from plant absorption, soil erosion, and dissolved P in runoff.

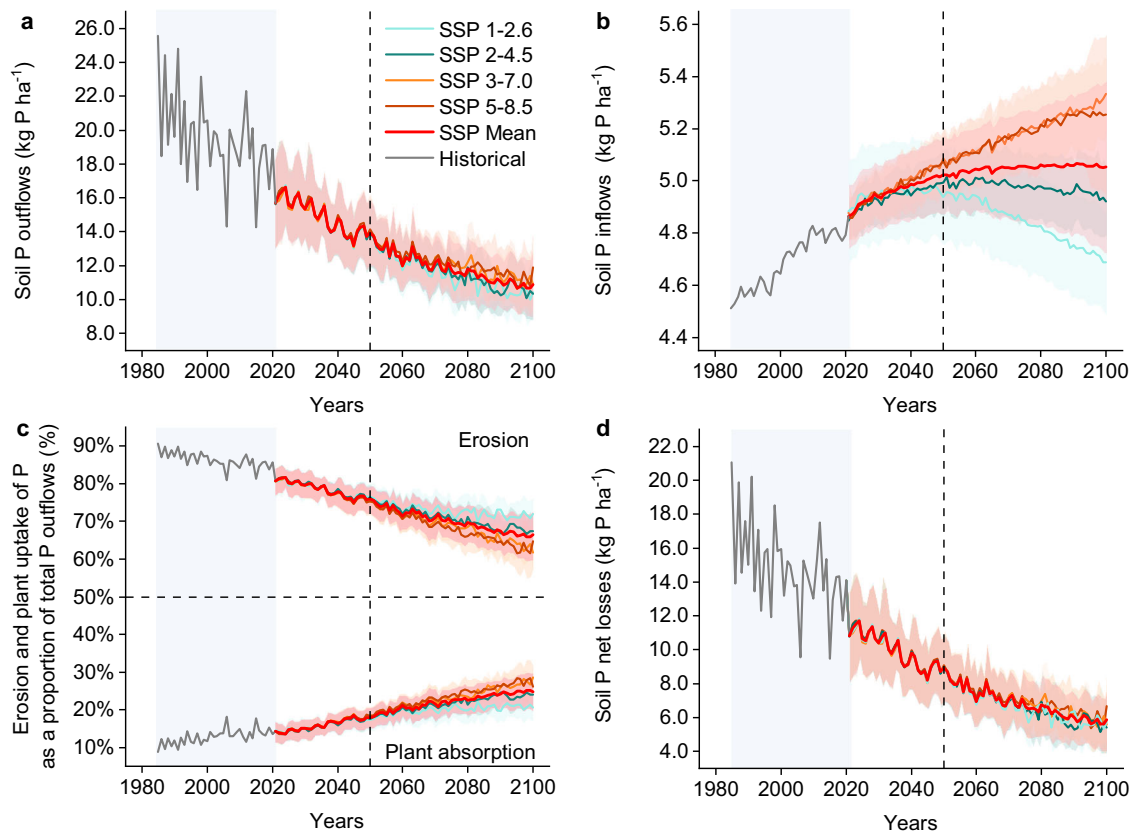


Fig. 5 | Trends in the soil P budget for the time period 2021–2100. a Soil P outflows. **b** Soil P inflows. **c** Erosion and plant uptake of P as a proportion of total P outflows. **d** Soil P net losses. The projected P dynamics were derived under the SSP1-2.6, SSP2-4.5, SSP3-7.0, and SSP5-8.5 future climate scenarios. The SSP2-4.5 and SSP5-8.5 scenarios were applied to predict future soil P flows from 27 CMIP6 global climate models, whereas the SSP1-2.6 and SSP3-7.0 scenarios were applied to

predict future soil P flows from 23 CMIP6 global climate models. The shading represents the standard deviation calculated for the corresponding 23/27 CMIP6 global climate models in each scenario. The black line shows the historical soil P budget data. The soil P outflows from erosion represent the sum of P losses from water and wind erosion. The results of the Mann–Kendall and change point tests show that the change point for the soil P budget is around 2050.

sources of material for wind erosion⁴¹. Dust aerosols can easily enter the middle and upper troposphere and be transported for long distances over East Asia and the Pacific Ocean due to a combination of the high terrain and intense atmospheric activities over the Tibetan Plateau⁴².

Potential scarcity of soil P by 2100

Our results highlight that the outflow of soil P will be higher than the inflow of soil P throughout the 21st century, although the loss of soil P gradually decreases under the SSP1-2.6, SSP2-4.5, SSP3-7.0 and SSP5-8.5 scenarios (Fig. 5a, b and Supplementary Fig. 12). In general, the future outflow of soil P in the alpine permafrost region is still dominated by erosion and absorption by plants (Fig. 5c), whereas the amounts of P outflow from human consumption and dissolved P in runoff are relatively low (Supplementary Fig. 13). The accumulation of biomass increases the P demand of plants under improved growth conditions for alpine plants (caused by warming, humidification and CO₂ enrichment) and extension of the length of the growing season^{21,43}. During the next few decades, the amount of soil P absorbed by plants may become gradually closer to the outflow of soil P caused by erosion and become a non-negligible cause of soil P deficiency in permafrost areas.

The results of the change-point tests showed that soil P will continue to decrease rapidly from the 2020s to the 2050s, with an average rate of 10.0 kg P ha⁻¹ yr⁻¹ (Fig. 5d). The projected net loss of soil P will then gradually slow down, with the mean rate decreasing to 6.8 kg P ha⁻¹ yr⁻¹ by the end of the 21st century (Fig. 5d), mainly due to a decrease in the amount of P outflow via erosion. The predicted mean

cumulative loss of the SPS for the four scenarios by the end of this century is 152.3 Tg P (Supplementary Fig. 14), which is just 20.3% of the 1980s stock, and thus highlights a serious challenge for future nutrient management and sustainable development in permafrost regions.

Implications and actions

Compared with previous P budgets^{2,11,19,20,24,44}, the challenge of P scarcity is more concerning in permafrost areas. Large disparities between the inflows and outflows of P in permafrost regions impose constraints on the function of terrestrial and associated aquatic ecosystems, such as productivity, the maintenance of biodiversity, and C sequestration.

Arctic and alpine permafrost ecosystems are generally considered to be nitrogen (N) limited²¹, and the rapid loss of soil P could increase the risk of P limitation in permafrost regions. Particularly, soil AP in the grassland ecosystem (occupying the largest area of the Tibetan Plateau) also decreased significantly, indicating that the soil P supply became insufficient (Supplementary Discussion 2). During the last few decades, an enhanced supply of available N in soils derived from the release of originally frozen N or accelerated N mineralization has been observed with climate warming or the thawing of permafrost^{21,45,46}. This imbalance in the availability of soil N and P may have a profound impact on the plant productivity and species diversity of terrestrial ecosystems by affecting the metabolism, growth rates, and reproduction, and therefore the life histories and competitiveness, of various microbes and plants^{27,47,48}. Consistent with this assumption, recent manipulation studies in alpine permafrost grasslands have suggested that increasing the availability of soil N can exacerbate P deficiency due to the unbalanced nutrient inputs⁴⁹. The soil P status has become the

key constraining factor regulating the gross primary productivity of permafrost and net ecosystem productivity¹⁴.

Large amounts of soil P are transferred from the permafrost to adjacent lakes and rivers, followed by transport to the coastal oceans²⁹, contributing to the potential risk of decreasing biodiversity and the production of algal blooms, and thereby threatening the health of the environment. The global losses of P from the land to freshwater bodies have doubled in the last century⁵⁰. There is a broadly articulated expectation that the thawing of permafrost will increase the transport of nutrients to aquatic networks under warming conditions³⁹. Although observational data have confirmed that most permafrost lakes show low rates of eutrophication, phytoplankton concentrations, and turbidity⁵¹, some lakes have experienced a decline in water quality and changes in their algal communities in recent years^{52,53}. For instance, previous studies found that total P concentrations in 7 lakes have exceeded the eutrophication threshold set by the OECD ($>35 \text{ mg L}^{-1}$)^{52,54} as well as exhibited a significant increasing trend for both prokaryotic and eukaryotic microorganisms over the past several decades⁵³. At the same time, the flux of P to water bodies has been found to alter the global C cycle¹²—for example, more productive aquatic ecosystems are hotspots of methane delivery to the atmosphere and store more organic C in permafrost riverbeds⁵⁵ and thermokarst lakebed sediments^{56,57}. A model simulation study suggested that increasing the P loading in lakes and impoundments will increase their methane emissions by up to 30–90% over the next century⁵⁸, and thus affect the trajectory of ecosystem C fluxes and exacerbate global climate change.

These model-prediction data imply that reducing the rapid loss of soil P is an urgent task in permafrost regions. At present, however, sustainable P management strategies are absent in these regions, as well as at the global scale. By the end of 2020, more than 500 scientists had signed a Call for International Action on Phosphorus, a petition calling on governments to support addressing the P emergency by coordinating action across five key sectors (agriculture, food consumption and production, waste management, mineral resource management, and aquatic resource management)¹². In 2022, the Our Phosphorus Future 50:50:50 Goal helped raise the profile of sustainable P management, calling for a 50% reduction in global P pollution and a 50% increase in the recycling of P lost in residues and wastes by 2050¹⁷. Although reducing the anthropogenic demand for P by avoiding the excess consumption of products and biomass energy (e.g., burning livestock dung and firewood) could improve the return of nutrients to the soil and compensate for some of the outflow of soil P in permafrost regions, it is difficult to achieve this goal. Nevertheless, soil and water conservation, an approach beyond these five key sectors, needs to be taken into consideration because of the high rate of P loss caused by erosion expected until 2050.

Agricultural practices may be able to reduce P loss by adopting conservation agriculture, sustainable farming practices, increasing the utilization of animal manure, or using management systems with increased use of residue inputs²⁴. However, in the long-term, a reduction in P losses through mitigating soil erosion (e.g., mulching, increased vegetation cover, intercropping and conservation agriculture), will be the most effective approach, and it will simultaneously enhance soil health, the general nutritional status of the soil (e.g., P and N), and water retention capacity¹¹. Although leguminous plants will mainly improve the N rather than P status of the soil, a recent review found that leguminous crops can utilize less accessible forms of P under P-deficient conditions via several mechanisms, including shaping a more refined root structure, releasing root exudate, and strengthening the connection with mycorrhizae⁵⁹. Alfalfa (*Medicago sativa* L. Alfking), a leguminous plant, is a high-quality forage type widely cultivated on the Tibetan Plateau⁶⁰, and thus growing/intercropping with alfalfa may be one of the effective ways to alleviate P limitation in cropland.

Limitations and future improvements

Although this study presents a temporal and spatial summary of P cycles across the alpine permafrost regions of the Tibetan Plateau from the 1980s to the 2020s, the flow quantification methods and datasets are not without their limitations.

There may have been some subtle changes in soil types over the past three decades. For example, afforestation, conversion of cropland to forest and grassland, and an upward shift in forest lines could result in interconversion of ecosystems and soil types on the Tibetan Plateau. The lack of continuous, high-precision data on spatial soil types may have led to some bias in our estimation of historical SPS changes.

The annual soil P concentration can provide precise data for estimating the SPS and improving the accuracy of the MPFE model. However, annual survey sampling for such a large area is very difficult because of the huge challenges in terms of labor and experimental costs. We used a space-for-time substitution method to interpolate the soil P concentration of missing years from the 1980s to 2020s, which may translate to discrepancies with the actual soil P concentration for a given year.

Our analysis presents a potential soil P crisis in the Tibetan alpine permafrost region, but the P cycle process is extremely complex, with both climatic factors (i.e., warming and humidification) and human activities possibly causing potential prediction uncertainties. For instance, the warming climate of the Tibetan Plateau is expected to enhance mineral weathering and may potentially promote the availability of soil P, while increasing precipitation (in both amount and magnitude) is expected to have negative impacts on SPD by accelerating water erosion (Supplementary Fig. 15). Some studies have found that plants can alleviate the limitation of P by promoting mycorrhizal symbiosis⁵⁹, activating mineral-bound P and uplifting P (biological pumping) from the deep soil layer⁶¹. It is very difficult for our model to capture these complex climate feedback mechanisms or ecological processes. Although the overall lower intensity of human activities has a relatively small impact on soil P changes (Supplementary Fig. 15), the local construction of highways/railways and mining may increase surface disturbances⁶², thereby accelerating erosion and the migration rate of P. For those variables, regional-scale data are not yet available for the Tibetan Plateau, which may also cause potential prediction uncertainties.

It should be pointed out that the relative importance of P and other resource limitations (e.g., N and water) varies under different soil degradation scenarios. For example, substantial soil P was translocated to plant biomass (grassland root and forest biomass), with the soil remaining well-preserved, and P limitation may become intense in the presence of a continuous decline in soil P. If soils are completely lost and new soil formation begins from bedrock, however, P availability may increase due to the weakened soil shielding effect and increased rock weathering caused by the frequent freeze–thaw effect⁶³, thereby leading to N and water possibly becoming more limiting factors.

The analysis presented in this paper is a systematic attempt to assess the historical changes in soil P pools and the key flows of P in permafrost regions using a unique combination of a soil resampling method and a modified process-balanced model, but both the methodology and spatial resolution of the MPFE model need additional work. For instance, the soil AP varies greatly in different months and seasons in permafrost areas due to the strong freeze–thaw effect^{64,65}. Therefore, high-temporal-resolution soil AP data need to be incorporated into the MPFE model in the future. Furthermore, due to the large differences stemming from the inefficient conversion from feed to meat (less than 10%, compared to 30% for crop production), changes in dietary structure across the Tibetan Plateau may lead to changes in P demand¹⁸. More accurate data on eating preferences and populations need to be incorporated into the MPFE model in the future.

Despite these limitations, we believe the conclusions of the present study broadly reflect the temporal trends of P cycle dynamics

across the alpine permafrost regions of the Tibetan Plateau. Moreover, this study provides a useful framework for future quantitative analysis of the P biogeochemical cycle.

Methods

Study area

The Tibetan Plateau, with an average altitude higher than 4000 m, covers the whole of the Tibet Autonomous Region and Qinghai Province, some of Gansu, Sichuan, and Yunnan provinces, and the Xinjiang Uygur Autonomous Region. The Tibetan Plateau covers the area (25.99–39.82°N, 73.50–104.67°E) (Supplementary Fig. 1). The Tibetan permafrost accounts for 75% of the area of alpine permafrost in the northern hemisphere⁶⁶. The Tibetan Plateau has experienced significant increases in the mean annual temperature, by 0.4 °C decade⁻¹⁶⁷, and precipitation has also shown a general upward trend during the last three decades⁴³. An increase in warming, moisture-induced thawing of the permafrost, and increased erosion have all been reported in recent decades^{38,39}. The two dominant natural ecosystems on the Tibetan Plateau are alpine grassland and forest⁶⁸. The main herbaceous species in the alpine grassland are *Kobresia pygmaea*, *Kobresia littledalei*, *Stipa purpurea*, and *Stipa glareosa*⁶⁹. The main woody species include *Abies georgei* var. *Abies likiangensis*, *Picea crassifolia*, *Abies faxoniana*, *Picea brachytyla* and *Betula albo-sinensis*⁷⁰. The croplands are mainly located in the gullies and valleys of Huangshui, Yarlung Tsangpo River, Lancang River, Niyang River, Nianchu River, Yalong River, and Shiquan River⁷¹. As important ecological protection areas and key agricultural production areas across the Tibetan Plateau, they provide important guarantees for local grain self-sufficiency⁷². The main grain crops are the two most common crops on the plateau—namely, highland barley and wheat. Following the World Reference Base for Soil Resources classification, the major soil types in alpine grasslands are *humic cambisols* and *haplic xerosols*, while forests are largely characterized by *humic cambisols*, *orthic luvisol*, and *dystric podzolusols*, and croplands by *haplic kastanozems* and *gelic leptosols*⁷³.

Urbanization on the Tibetan Plateau has been relatively slow during the last three decades (Supplementary Figs. 16 and 17). The Tibetan Plateau is still dominated by natural ecosystems, although the impervious area has increased from 5454 to 15,997 ha during the last three decades. In 2020, the impervious area of the Tibetan Plateau accounted for <0.007% of the plateau (Supplementary Fig. 17). Historically, farmers and herders have had their own unique lifestyles, consuming mainly beef, mutton, milk, fur, and grain. The dung from livestock (e.g., yaks, yellow cattle, Pien Niu, goats, and sheep) is burned as fuel for cooking and heating in the grassland and cropland areas, whereas firewood is burned for cooking and heating in the forested areas^{74,75}. There are few areas of intensive pasture and most farmers are self-sufficient and follow traditional grazing and farming patterns.

Field resampling and laboratory measurements

We compiled a broad-scale repeat-sampling dataset based on two multi-year field campaigns in the 1980s and the 2020s to detect any changes in the SPD and stock across the alpine permafrost regions of the Tibetan Plateau. Historical soil data were obtained from the Second National Soil Inventory of China and the First Tibetan Plateau Scientific Expedition Program. The data from the Second National Soil Inventory of China were compiled by the Agriculture and Animal Husbandry Bureau or the Agricultural Bureau, whereas the data from the First Tibetan Plateau Scientific Expedition Program were compiled by the Tibetan Plateau Research Team, Chinese Academy of Sciences, during the 1980s (Supplementary Table 1).

Historical data for the physical and chemical properties of soils are reported in individual monographs for each province, city, and county. These monographs contain soil data of the typical profiles of different soil series and record detailed information, including the

geographical location, records of landmarks, parent material, soil type, topographic features, land use type, vegetation type, the dominant species, and the physicochemical properties of each soil genetic horizon. The original soil P dataset comprised 605 plots in the 1980s. As a result of practical constraints (e.g., natural hazards, road rebuilding, and human disturbance; see Supplementary Method 1), a total of 255 perfectly matched resampling plots were obtained (Supplementary Fig. 1). Frequency distribution analysis of SPD revealed similar means between the original and resampled plots. A mixed-effects model further confirmed no significant difference between the two datasets ($P > 0.05$). The distribution and representativeness of the plots are depicted in Supplementary Fig. 2. Historical data in the 1980s were recorded from 131 counties across the Tibetan Plateau, and resampling plots were obtained from 93 counties in the 2020s, accounting for 71% of the total 131 counties (Supplementary Fig. 1b). To further evaluate the accuracy of our plots, we compared all the plots with other independent references. We made secondary use of different maps, including vegetation-type maps, soil-type maps, topographic maps (elevation, slope, and terrain), land-use maps (residential areas, rivers, and lakes), road maps, and administrative-boundary maps that were developed before 1990s (more details see Supplementary Method 1). In addition, we also consulted several staff who participated in the 1980s campaign to determine the exact locations of the sampling plots. Plots in close proximity to electric power lines, roads, railways, or drainage ditches were avoided. These plots were set throughout the geographical extent of alpine forests, grasslands and cropland, covering a wide range of climates (mean annual temperature: -12.6–14.3 °C; mean annual precipitation: 22.4–1299.5 mm), vegetation characteristic (net primary productivity: 6.1–1173.7 g C m⁻² yr⁻¹; normalized difference vegetation index (NDVI): 0–0.8), soil properties (soil P concentration: 0.2–1.6 g kg⁻¹; soil AP concentration: 0.4–97.6 mg kg⁻¹) across the plateau. The topography, parent material, soil type, vegetation type, dominant species, and management strategies of the 255 resampling plots did not change during the intra-sampling period.

We randomly set up three (20 × 20 m) quadrats at intervals of 10 m and collected soil samples from the center of each quadrat for each plot (Supplementary Fig. 1c). At each sampling quadrat, a square pit covering an area of (1 × 1 m) was dug and a rule was placed inside the pit along the profile (repeated three times). We took three soil cores in each plot to generate descriptions of their vertical properties (e.g., layering, color, and texture for each layer) for comparisons with those from the 1980s. The consistency between each layer of the profile in the 2020s and the historical record was the key piece of evidence used to determine whether the soil sample was collected correctly. Undisturbed soil samples were collected from different soil depth intervals according to the soil genetic horizon. A 2 kg sample of each soil layer was placed into a Ziploc bag and labels were affixed inside and outside the bag, recording the profile number, location, depth, and other information. To test the soil bulk density, 100 cm³ steel cylinders were pushed into the soil profile with the center of the cylinder aimed at the central depth of each soil genetic horizon. If the target soil genetic horizon was thinner than the diameter of the steel cylinders, the adjacent layers shared the soil bulk density data of the thicker soil genetic horizon. Where large stones and tree roots were present, we moved the square pit horizontally (for all soil genetic horizons) until we could successfully collect soil samples from along the whole profile.

The soil samples collected in the 2020s were air-dried to a constant weight in a ventilated room (-15–20 °C). The soil samples were then ground and passed through 2 and 0.149 mm sieves after any stones, plant litter, and roots had been removed. The P concentration of each soil sample was determined by the molybdenum antimony resistance to colorimetric method⁷⁶, and the soil AP concentration was determined by the NaHCO₃ extraction/Mo-Sb colorimetric method⁷⁷.

The two analysis methods were identical to the methods used in the 1980s. The samples used to determine the bulk density were dried to constant weight in an oven at 105 °C. The mean P concentration and bulk density determined for three repeat samples from each soil layer were used in all further calculations. We selected the soil horizon corresponding to a thickness of 30 cm, which includes most of the plant roots and is the most active soil layer in the biogeochemical cycle of P⁷⁸. Although there was a significant positive correlation between the P concentration in the two time periods at the same plot, the soil P concentration decreased significantly from the 1980s to the 2020s (Supplementary Fig. 18).

The SPD in the top 30 cm was calculated for each soil profile using the following equation:

$$\text{SPD} = \frac{\sum_{i=1}^n T_i \times \text{BD}_i \times \text{SPC}_i}{H} \quad (1)$$

where SPD is the SPD (kg P ha⁻¹), T_i is the layer thickness (cm), BD is the bulk density (g cm⁻³), SPC is the soil P concentration (g P kg⁻¹), i is a particular soil layer, and H is the number of profile layers within 30 cm.

For each resampled plot, the change in the SPD was calculated as

$$\Delta\text{SPD} = \text{SPD}_{2020\text{s}} - \text{SPD}_{1980\text{s}} \quad (2)$$

where ΔSPD represents the change in the SPD of the 0–30 cm depth soil layer during the last three decades (kg P ha⁻¹), $\text{SPD}_{2020\text{s}}$ is the SPD of the 0–30 cm depth soil layer obtained in the 2020s, and $\text{SPD}_{1980\text{s}}$ is the SPD of the 0–30 cm depth soil layer obtained in 1980s. The calculation method for the soil AP density is consistent with that used for the SPD.

The soil P stock (SPS) was calculated according to the distribution area of different soil types and their corresponding SPD in grassland, forest, and cropland ecosystems because the SPD varies significantly in different soil types and even in the same soil type in different ecosystems. We then added the SPS of the three ecosystems to obtain the total SPS across the Tibetan Plateau. The soil type map was obtained from China's soil atlas (scale 1:50,000)⁷⁹, SoilGrid (250 m; <https://www.soilgrids.org/>), and the FAO (50 km; <https://www.fao.org/>). An ensemble calculation of the SPS was adopted to reduce the uncertainty caused by the three different resolutions of these soil maps. The vegetation maps of the 1980s⁶⁸ and 2020s⁸⁰ were obtained from China's vegetation atlas (scale 1:1,000,000). The grassland ecosystem includes alpine meadow, steppe, desert, and cushion vegetation.

We compared the results of changes in the SPS during the two time periods. The change in SPS was calculated as

$$\Delta\text{SPS} = \text{SPS}_{2020\text{s}} - \text{SPS}_{1980\text{s}} \quad (3)$$

where ΔSPS represents the change in SPS of the 0–30 cm depth soil layer during the last three decades (kg P), $\text{SPS}_{2020\text{s}}$ is the SPS of the 0–30 cm depth soil obtained in the 2020s, and $\text{SPS}_{1980\text{s}}$ is the SPS of the 0–30 cm depth soil layer obtained in the 1980s.

Simulations of P flow in ecosystems

Our general conceptual framework for the soil P budget in grassland, forest and cropland ecosystems is based on the principle of mass balance (Fig. 1). The MPFE consists of the main key P inflow and outflow subsystems, including weathering, atmospheric deposition, fertilizer, absorption by plants, deposition via livestock excretions, litter return, livestock feed, livestock, forest and grain products, the burning of livestock excretion products (animal dung) for fuel, and soil erosion (Supplementary Method 2 and Supplementary Table 2). This framework has previously been widely applied to P flows on national and global scales^{1,11,32,81,82}. Similar to conventional modeling approaches, we

compared our calculations of the main P inflow and outflow subsystems with those of other studies (Supplementary Tables 3–5). A notable difference between this work and previous studies is that the soil P data were repeatedly measured in situ for the two time periods to verify and improve the accuracy of the MPEF. In particular, we compared the observations and simulations of the change in the SPD between final and first years of observations (see Statistical analyses, below). The net change in soil P is the P inflow minus the P outflow:

$$\text{Soil P budget} = \text{Soil P inflow} - \text{Soil P outflow} \quad (4)$$

$$\begin{aligned} \text{Soil P inflow} = & \text{P released from weathering} + \text{Atmospheric P deposition} \\ & + \text{P deposition via excretion} + \text{P return from plant litter} \\ & + \text{P fertilizer} \end{aligned} \quad (5)$$

$$\begin{aligned} \text{Soil P outflow} = & \text{P absorption by plants} + \text{P loss via erosion} \\ & + \text{Loss of dissolved P} \end{aligned} \quad (6)$$

Briefly, the inputs of P from weathering, atmospheric deposition and fertilizer are the P inflow subsystems, whereas the P loss from soil erosion (particulate P) and runoff (dissolved P) are the P outflow subsystems. However, the calculations for the plant-related P flows are more complex and include the net accumulation by plants, the return of plant litter to the soil, feeding by livestock, the deposition of livestock excretions, and human consumption (e.g., livestock, forest and grain products, and the burning of livestock excretion products for fuel)^{19,82} (Supplementary Figs. 19–21, Supplementary Data 1, 2). All the inflows and outflows of P were calculated at a resolution of an 8 × 8 km grid and are given in Supplementary Method 2.

Supplementary Table 3 compares the estimates of the main plant-related P flows on the Tibetan Plateau with those reported by other researchers. Although it is not easy to compare all the results obtained in this study with those reported previously due to differences in the system boundaries, approaches, and scope, it is possible to compare some of the flows calculated here with a few other studies conducted on the Tibetan Plateau and in China and Asia. Most of our modeled P flows were of the same order of magnitude as previous P flows (Supplementary Table 3). However, previous studies found larger amounts of P stored in livestock products, primarily due to the large number of yak and sheep in the alpine meadow ecosystem, whereas our study covered all types of alpine grasslands. The sparse population, low vegetation coverage and small number of livestock in the central and western areas of the plateau (i.e., the alpine steppe and alpine desert) resulted in a low P density for livestock products per unit area. The carcass weight, which is the weight of an animal after slaughter and the removal of the fur, head, and genitourinary organs, is the common indicator of livestock meat production. In the present study, however, the total amount of P in livestock products was the sum of the amount of P in meat, milk, and livestock byproducts (blood, adipose tissue, skeleton, viscera, digestive content, and skin hair). There are large differences in the P concentration in different fractions, such as the skull, gut, and blood¹. Such differences in calculation methods may lead to differences in the P outflow of livestock products.

The Revised Universal Soil Loss Equation (RUSLE) and the Revised Wind Erosion Equation (RWEQ) models were used to calculate the erosion of soil by water and wind, respectively (Supplementary Method 2). To verify the accuracy of the estimation of the RUSLE and RWEQ models, our results were compared with other measurements (e.g., model simulation, isotopic tracing, and sand collection from the field). Our estimates of the P flows caused by erosion were of the same order of magnitude as previous P flows (Supplementary Table 4). For water erosion, the calculated potential soil P loss in this study was well

within the range of published on-site riverine P exports for the Yangtze, Yellow, Lancang, Nujiang, Yarlung Tsangpo, Heihe, and Shule rivers (Supplementary Table 5). Although the riverine P loads of a few hydrological stations may not completely cover the P soil erosion status of the whole basin, they can provide an important reference for verifying the transport of P by sediments. Although the P transported from soils might be redeposited within water catchments (i.e., wetlands, lakes, ponds, riparian zones or buffer strips), the potential threats of P loss from soils are not reduced¹¹.

Future scenario for the time period 2021–2100

Future climate data projected by 27 global climate models (GCMs) of the Coupled Model Intercomparison Project Phase 6 (CMIP6) from 2021 to 2100 were downloaded from the World Climate Research Program (WCRP) dataset (<https://esgf-node.llnl.gov/search/cmip6/>). The raw GCMs from the WCRP dataset were at low spatial and temporal resolutions and therefore downscaling and bias-correction methods were used to generate the site-scale daily datasets⁸³.

Four SSP scenarios (including the SSP1-2.6, SSP2-4.5, SSP3-7.0 and SSP5-8.5 future climate scenarios of the CMIP6 models) were selected for projecting future soil P budgets (Supplementary Table 7). The SSP2-4.5 and SSP5-8.5 scenarios were applied to predict future P flows on the Tibetan Plateau from the 27 GCMs of CMIP6—namely, ACCESS-CM2, ACCESS-ESM1-5, BCC-CSM2-MR, CanESM5, CanESM5-CanOE, CNRM-CM, CNRM-CM6-1-HR, CNRM-ESM, EC-Earth3, EC-Earth3-Veg, FGOALS-g3, GFDL-ESM4, GISS-E2-1-G, INM-CM4-8, INM-CM5-0, IPSL-CM, MIROC6, MIROC-ES2L, MPI-ESM1-2-HR, MPI-ESM1-2-LR, MRI-ESM, UKESM1-0-LL, CMCC-CM2-SR5, CIESM, GFDL-CM4, MRI-ESM2-0 and NESM3. The SSP1-2.6 and SSP3-7.0 scenarios do not include the CMCC-CM2-SR5, CIESM, GFDL-CM4, and NESM3 models. The data were integrated using the multi-model ensemble method to reduce the uncertainty caused by an individual GCM. The average result from multiple GCMs is widely used in climate projections based on the assumption that the errors tend to cancel each other out if the GCMs are independent^{84–86}.

Future population data were derived from gridded population and economy datasets under the four SSP scenarios⁸⁷. To verify the accuracy of future predictions under each scenario, we standardized the meteorological (1985–2020) and population (2010–2020) data during the common period. Based on the linear relationship between the data series before and after this treatment, we converted the modeled result to a historical result and then scaled the future data accordingly⁸⁸.

Statistical analyses

Descriptive statistics included the frequency distributions, means, and 95% confidence intervals of the means of the SPD at a soil depth of 0–30 cm for both time periods. The relationship between the SPD in the 1980s and 2020s was analyzed using the ordinary least-squares (OLS) regression model. The temporal changes in SPDs were examined with linear mixed-effects models using the *lme4*⁸⁹ and the *lmerTest*⁹⁰ packages in R version 4.2.1, in which the fixed effect was the sampling period and the random effect was the sampling plot. The effects of the sampling period on the SPD were considered significant if $P < 0.05$. The homoscedasticity and normality of the residuals were tested before the linear mixed modeling analyses and in-normal transformation was conducted where necessary. The historical trend of the outflow and inflow of the SPD from the 1980s to the 2020s was analyzed by the OLS regression model.

To test the accuracy of the dynamic model for P, a simulation vs. observation comparison of the change in the SPD between the observations in the 1980s and the 2020s was analyzed at both the sampling plot and county scale. First, the OLS fit of the linear equation was applied to calculate the relationship between the simulated vs. observational SPD data for the two sampling periods. The coefficient

of determination can reflect the correlation of the SPD between the simulated and actual sampling data. Second, the slope of the fitted equation was compared with the 1:1 line using the *tidyverse* package to determine whether the simulated and observed data increased or decreased in equal proportions⁹¹. A mixed-effects model was then conducted using the *lme4*⁸⁹ and *lmerTest*⁹⁰ packages in R version 4.2.1 to test for possible random effects due to the measurements being made by different methods across sampling plots and counties. The effects of different methods on the SPD were considered significant if $P < 0.05$. Through these three verification methods, the model was shown to roughly match the in situ decrease in soil P on the Tibetan Plateau over the last three decades.

Predicted trends in the soil P budget and their associated change points for the time period 2021–2100 were analyzed using the Mann–Kendall and change-point tests using the *trend*⁹² and *cpm*⁹³ packages, respectively, in R version 4.2.1. The Kolmogorov–Smirnov test was used to extract the change points because the data did not conform to a Gaussian distribution.

Data availability

All data are available in the article and its Supplementary Information. Source data are provided with this paper. The daily rainfall, daily temperature and daily wind speed are available at <https://data.cma.cn/>; the Daily snow depth is available at <https://data.tpdac.cn/home>; the NDVI is available at <http://www.csdata.org>; the N deposition is available at <https://doi.org/10.3334/ORNDAAC/1220>; the ANPP is available at <http://www.glass.umd.edu/Download.html>; the DEM is available at <https://www.jpl.nasa.gov/missions/shuttle-radar-topography-mission-srtm>; the LUCC (land-use and land-cover change) is available at <https://www.earth-system-science-data.net/>; the soil property data (e.g., sand, silt, clay and SOC) are available at <https://www.soilgrids.org/>; the CaCO₃ data are available at <https://gaez.fao.org/pages/hwsd>; the CNRD v1.0 dataset is available at <https://data.tpdac.cn/zh-hans/data/8b6a12c7-c8f9-465a-b449-852fbff51853/>; and the future population data are available at <https://geography.nuist.edu.cn/2019/1113/c1954a147560/pagem.psp>. The SPD data and the geographical/environmental characteristics for the resampling plots are available in Supplementary Data 3.

Code availability

Figures were created in Microsoft PowerPoint software, R 4.2.1, MATLAB R2022a, Adobe Acrobat DC, and ArcGIS 10.6 (<https://www.esri.com/>). The data analysis codes have been deposited in the figshare database at <https://figshare.com/articles/code/29134574>.

References

- Sattari, S. Z., Bouwman, A. F., Rodriguez, R. M., Beusen, A. H. W. & van Ittersum, M. K. Negative global phosphorus budgets challenge sustainable intensification of grasslands. *Nat. Commun.* **7**, 10696 (2016).
- Sattari, S. Z., Bouwman, A. F., Giller, K. E. & van Ittersum, M. K. Residual soil phosphorus as the missing piece in the global phosphorus crisis puzzle. *Proc. Natl. Acad. Sci. USA* **109**, 6348–6353 (2012).
- Sitters, J., Kimuyu, D. M., Young, T. P., Claeys, P. & Venterink, H. Negative effects of cattle on soil carbon and nutrient pools reversed by megaherbivores. *Nat. Sustain.* **3**, 360–366 (2020).
- Quigg, A. et al. The evolutionary inheritance of elemental stoichiometry in marine phytoplankton. *Nature* **425**, 291–294 (2003).
- Zhang, T., Barry, R. G., Knowles, K., Heginbottom, J. A. & Brown, J. Statistics and characteristics of permafrost and ground-ice distribution in the Northern Hemisphere. *Polar Geogr.* **31**, 47–68 (2008).
- He, X. J. et al. Global patterns and drivers of soil total phosphorus concentration. *Earth Syst. Sci. Data* **13**, 5831–5846 (2021).

7. Slater, A. G. & Lawrence, D. M. Diagnosing present and future permafrost from climate models. *J. Clim.* **26**, 5608–5623 (2013).
8. Peterson, B. J. et al. Trajectory shifts in the Arctic and subarctic freshwater cycle. *Science* **313**, 1061–1066 (2006).
9. Abbott, B. W., Jones, J. B., Godsey, S. E., Larouche, J. R. & Bowden, W. B. Patterns and persistence of hydrologic carbon and nutrient export from collapsing upland permafrost. *Biogeosciences* **12**, 3725–3740 (2015).
10. Hobbie, S. E. et al. Contrasting nitrogen and phosphorus budgets in urban watersheds and implications for managing urban water pollution. *Proc. Natl. Acad. Sci. USA* **114**, 4177–4182 (2017).
11. Alewell, C. et al. Global phosphorus shortage will be aggravated by soil erosion. *Nat. Commun.* **11**, 4546 (2020).
12. Brownlie, W. J. et al. Global actions for a sustainable phosphorus future. *Nat. Food* **2**, 71–74 (2021).
13. Elser, J. J. et al. Sustained stoichiometric imbalance and its ecological consequences in a large oligotrophic lake. *Proc. Natl. Acad. Sci. USA* **119**, e2202268119 (2022).
14. Yang, G. B. et al. Phosphorus rather than nitrogen regulates ecosystem carbon dynamics after permafrost thaw. *Glob. Change Biol.* **27**, 5818–5830 (2021).
15. Zimov, S. A., Schuur, E. A. G. & Chapin, F. S. Permafrost and the global carbon budget. *Science* **312**, 1612–1613 (2006).
16. Barbieri, P., MacDonald, G. K., Bernard de Raymond, A. & Nesme, T. Food system resilience to phosphorus shortages on a telecoupled planet. *Nat. Sustain.* **5**, 114–122 (2022).
17. Brownlie, W. J., Sutton, M. A., Heal, K. V., Reay, D. S. & Spears, B. Our Phosphorus Future: Towards Global Phosphorus Sustainability. 371 (Centre for Ecology & Hydrology, Edinburgh, UK, 2022).
18. Chen, M. P. & Graedel, T. E. A half-century of global phosphorus flows, stocks, production, consumption, recycling, and environmental impacts. *Glob. Environ. Chang.* **36**, 139–152 (2016).
19. Bouwman, L. et al. Exploring global changes in nitrogen and phosphorus cycles in agriculture induced by livestock production over the 1900–2050 period. *Proc. Natl. Acad. Sci. USA* **110**, 20882–20887 (2013).
20. Liu, X. et al. Intensification of phosphorus cycling in China since the 1600s. *Proc. Natl. Acad. Sci. USA* **113**, 2609–2614 (2016).
21. Kou, D. et al. Progressive nitrogen limitation across the Tibetan alpine permafrost region. *Nat. Commun.* **11**, 3331 (2020).
22. Prietzel, J., Zimmermann, L., Schubert, A. & Christophel, D. Organic matter losses in German Alps forest soils since the 1970s most likely caused by warming. *Nat. Geosci.* **9**, 543–548 (2016).
23. Bellamy, P. H., Loveland, P. J., Bradley, R. I., Lark, R. M. & Kirk, G. J. D. Carbon losses from all soils across England and Wales 1978–2003. *Nature* **437**, 245–248 (2005).
24. MacDonald, G. K., Bennett, E. M., Potter, P. A. & Ramankutty, N. Agronomic phosphorus imbalances across the world's croplands. *Proc. Natl. Acad. Sci. USA* **108**, 3086–3091 (2011).
25. Liu, Y., Villalba, G., Ayres, R. U. & Schroder, H. Global phosphorus flows and environmental impacts from a consumption perspective. *J. Ind. Ecol.* **12**, 229–247 (2008).
26. Smil, V. Phosphorus in the environment: natural flows and human interferences. *Annu. Rev. Energ. Env.* **25**, 53–88 (2000).
27. Peñuelas, J. et al. Human-induced nitrogen-phosphorus imbalances alter natural and managed ecosystems across the globe. *Nat. Commun.* **4**, 2934 (2013).
28. Mu, C. et al. Editorial: Organic carbon pools in permafrost regions on the Qinghai-Xizang (Tibetan) Plateau. *Cryosphere* **9**, 479–486 (2015).
29. Raymo, M. E. & Ruddiman, W. F. Tectonic forcing of late Cenozoic climate. *Nature* **359**, 117–122 (1992).
30. Yang, Y. H. et al. Stoichiometric shifts in surface soils over broad geographical scales: evidence from China's grasslands. *Glob. Ecol. Biogeogr.* **23**, 947–955 (2014).
31. Tian, L. M. et al. Variations in soil nutrient availability across Tibetan grassland from the 1980s to 2010s. *Geoderma* **338**, 197–205 (2019).
32. Ringeval, B. et al. Phosphorus in agricultural soils: drivers of its distribution at the global scale. *Glob. Change Biol.* **23**, 3418–3432 (2017).
33. Mutlutürk, M., Altındag, R. & Türk, G. A decay function model for the integrity loss of rock when subjected to recurrent cycles of freezing-thawing and heating-cooling. *Int. J. Rock. Mech. Min.* **41**, 237–244 (2004).
34. Hawkings, J. et al. The Greenland Ice Sheet as a hot spot of phosphorus weathering and export in the Arctic. *Glob. Biogeochem. Cycle* **30**, 191–210 (2016).
35. Wang, X. D. et al. Assessment on protection and construction of ecological safety shelter for Tibet. *Bull. Chin. Acad. Sci.* **32**, 29–34 (2017).
36. Yang, K. et al. Response of hydrological cycle to recent climate changes in the Tibetan Plateau. *Clim. Change* **109**, 517–534 (2011).
37. Shi, X. N. et al. The response of the suspended sediment load of the headwaters of the Brahmaputra River to climate change: Quantitative attribution to the effects of hydrological, cryospheric and vegetation controls. *Glob. Planet. Change* **210**, 103753 (2022).
38. Zhang, F. et al. Recent stepwise sediment flux increase with climate change in the Tuotuo River in the central Tibetan Plateau. *Sci. Bull.* **65**, 410–418 (2020).
39. Li, J. L. et al. Recent intensified erosion and massive sediment deposition in Tibetan Plateau rivers. *Nat. Commun.* **15**, 722 (2024).
40. Tank, S. E. et al. Recent trends in the chemistry of major northern rivers signal widespread Arctic change. *Nat. Geosci.* **16**, 789–796 (2023).
41. Teng, Y. M. et al. Spatiotemporal dynamics and drivers of wind erosion on the Qinghai-Tibet Plateau, China. *Ecol. Indic.* **123**, 107340 (2021).
42. Han, Y. X., Fang, X. M., Xi, X. X., Song, L. C. & Yang, S. L. Dust storm in Asia continent and its bio-environmental effects in the North Pacific: a case study of the strongest dust event in April, 2001 in central Asia. *Chin. Sci. Bull.* **51**, 723–730 (2006).
43. Wang, Y. F. et al. Grassland changes and adaptive management on the Qinghai-Tibetan Plateau. *Nat. Rev. Earth Env.* **3**, 668–683 (2022).
44. Reinhard, C. T. et al. Evolution of the global phosphorus cycle. *Nature* **541**, 386–389 (2017).
45. Keuper, F. et al. A frozen feast: thawing permafrost increases plant-available nitrogen in subarctic peatlands. *Glob. Change Biol.* **18**, 1998–2007 (2012).
46. Finger, R. A. et al. Effects of permafrost thaw on nitrogen availability and plant-soil interactions in a boreal Alaskan lowland. *J. Ecol.* **104**, 1542–1554 (2016).
47. Yuan, Z. Y. & Chen, H. Y. H. Decoupling of nitrogen and phosphorus in terrestrial plants associated with global changes. *Nat. Clim. Change* **5**, 465–469 (2015).
48. Peñuelas, J. & Sardans, J. The global nitrogen-phosphorus imbalance. *Science* **375**, 266–267 (2022).
49. Wang, Y. H. et al. Asymmetric response of aboveground and belowground temporal stability to nitrogen and phosphorus addition in a Tibetan alpine grassland. *Glob. Change Biol.* **29**, 7072–7084 (2023).
50. Beusen, A. H. W., Bouwman, A. F., Van Beek, L. P. H., Mogollón, J. M. & Middelburg, J. J. Global riverine N and P transport to ocean increased during the 20th century despite increased retention along the aquatic continuum. *Biogeosciences* **13**, 2441–2451 (2016).
51. Liu, C. et al. In-situ water quality investigation of the lakes on the Tibetan Plateau. *Sci. Bull.* **66**, 1727–1730 (2021).
52. Wu, Y. et al. Emerging water pollution in the world's least disturbed lakes on Qinghai-Tibetan Plateau. *Environ. Pollut.* **272**, 116032 (2021).

53. Ouyang, J. W. et al. Global warming induces the succession of photosynthetic microbial communities in a glacial lake on the Tibetan Plateau. *Water Res.* **242**, 120213 (2023).
54. Hart, B. T. Eutrophication of waters - monitoring, assessment and control - OECD. *Search* **15**, 50 (1984).
55. Zhang, L. W. et al. Significant methane ebullition from alpine permafrost rivers on the East Qinghai-Tibet Plateau. *Nat. Geosci.* **13**, 349–354 (2020).
56. Yang, G. B. et al. Characteristics of methane emissions from alpine thermokarst lakes on the Tibetan Plateau. *Nat. Commun.* **14**, 3121 (2023).
57. Walter, K. M., Edwards, M. E., Grosse, G., Zimov, S. A. & Chapin, F. S. Thermokarst lakes as a source of atmospheric CH₄ during the last deglaciation. *Science* **318**, 633–636 (2007).
58. Beaulieu, J. J., DelSontro, T. & Downing, J. A. Eutrophication will increase methane emissions from lakes and impoundments during the 21st century. *Nat. Commun.* **10**, 1375 (2019).
59. Franke, A. C., van den Brand, G. J., Vanlauwe, B. & Giller, K. E. Sustainable intensification through rotations with grain legumes in Sub-Saharan Africa: a review. *Agr. Ecosyst. Environ.* **261**, 172–185 (2018).
60. Cui, J. et al. Plant preference for NH₄⁺ versus NO₃⁻ at different growth stages in an alpine agroecosystem. *Field Crop. Res.* **201**, 192–199 (2017).
61. Lucas, Y. The role of plants in controlling rates and products of weathering: importance of biological pumping. *Annu. Rev. Earth Planet. Sci.* **29**, 135–163 (2001).
62. Chen, H. et al. Carbon and nitrogen cycling on the Qinghai-Tibetan Plateau. *Nat. Rev. Earth Env.* **3**, 701–716 (2022).
63. Hartmann, J., Moosdorf, N., Lauerwald, R., Hinderer, M. & West, A. J. Global chemical weathering and associated P-release - the role of lithology, temperature and soil properties. *Chem. Geol.* **363**, 145–163 (2014).
64. Zhou, L. L., Dong, H., Huang, D. H., Fan, H. M. & Jia, Y. F. Responses of available phosphorus in different slope aspects to seasonal freeze-thaw cycles in Northeast China. *Soil Res.* **203**, 104706 (2020).
65. Huang, D. H., Zhou, L., Fan, H., Jia, Y. & Liu, M. Responses of aggregates and associated soil available phosphorus, and soil organic matter in different slope aspects, to seasonal freeze-thaw cycles in Northeast China. *Geoderma* **402**, 115184 (2021).
66. Yang, M. X., Nelson, F. E., Shiklomanov, N. I., Guo, D. L. & Wan, G. N. Permafrost degradation and its environmental effects on the Tibetan Plateau: a review of recent research. *Earth Sci. Rev.* **103**, 31–44 (2010).
67. Pepin, N. et al. Elevation-dependent warming in mountain regions of the world. *Nat. Clim. Change* **5**, 424–430 (2015).
68. Zhang, X. S. *Vegetation map of the People's Republic of China (1:1,000,000)* (Geology Press, 2007).
69. He, J. S. et al. A test of the generality of leaf trait relationships on the Tibetan Plateau. *New Phytol.* **170**, 835–848 (2006).
70. Luo, T. X., Li, W. H. & Zhu, H. Z. Estimated biomass and productivity of natural vegetation on the Tibetan Plateau. *Ecol. Appl.* **12**, 980–997 (2002).
71. Duan, J., Wang, W. T., Xu, Y. & Ru, Y. X. Evolution and driving factors of grain supply and demand balance in the Qinghai-Tibet Plateau in recent 30 years. *Acta Ecol. Sin.* **44**, 1–16 (2024).
72. Wang, J., Guan, Y. J., Wang, H. Y. & Zhou, W. Identifying and monitoring of abandoned farmland in key agricultural production areas on the Qinghai-Tibet Plateau: a case study of the Huangshui Basin. *J. Environ. Manag.* **354**, 120380 (2024).
73. Lu, H. Y. et al. Distribution of carbon isotope composition of modern soils on the Qinghai-Tibetan Plateau. *Biogeochemistry* **70**, 273–297 (2004).
74. Xiao, Q. Y. et al. Indoor air pollution from burning yak dung as a household fuel in Tibet. *Atmos. Environ.* **102**, 406–412 (2015).
75. Jiang, L., Xing, R., Chen, X. P. & Xue, B. Rural household energy consumption of farmers in the Qinghai-Tibet Plateau. *Sci. Geogr. Sin.* **40**, 447–454 (2020).
76. Sommers, L. E. & Nelson, D. W. Determination of total phosphorus in soils-rapid perchloric acid-digestion procedure. *Soil Sci. Soc. Am. J.* **36**, 902–904 (1972).
77. Lu, R. K. *Soil and Agricultural Chemistry Analysis Method* (China Agriculture Science and Technique Press, 2000).
78. Jackson, R. B. et al. A global analysis of root distributions for terrestrial biomes. *Oecologia* **108**, 389–411 (1996).
79. Shi, X. Z. et al. Soil information system of China (SISChina) and its application. *Soils* **39**, 329–333 (2007).
80. Zhou, J. et al. Vegetation map of the Qinghai Tibet Plateau, <https://doi.org/10.11888/ Terre.tpd.300884>. (2023)
81. Bai, Z. H. et al. Nitrogen, phosphorus, and potassium flows through the manure management chain in China. *Environ. Sci. Technol.* **50**, 13409–13418 (2016).
82. Zhang, X. et al. Quantifying nutrient budgets for sustainable nutrient management. *Glob. Biogeochem. Cycle* **34**, e2018GB006060 (2020).
83. Liu, D. L. & Zuo, H. P. Statistical downscaling of daily climate variables for climate change impact assessment over New South Wales, Australia. *Clim. Change* **115**, 629–666 (2012).
84. Dai, A. G., Rasmussen, R. M., Ikeda, K. & Liu, C. H. A new approach to construct representative future forcing data for dynamic downscaling. *Clim. Dynam.* **55**, 315–323 (2017).
85. Hessel, A. E. et al. Past and future drought in Mongolia. *Sci. Adv.* **4**, e1701832 (2018).
86. Tebaldi, C. & Knutti, R. The use of the multi-model ensemble in probabilistic climate projections. *Philos. Trans. R. Soc. A* **365**, 2053–2075 (2007).
87. Huang, J. L. et al. Effect of fertility policy changes on the population structure and economy of China: from the perspective of the shared socioeconomic pathways. *Earth Future* **7**, 250–265 (2019).
88. Chen, F. et al. Southeast Asian ecological dependency on Tibetan Plateau streamflow over the last millennium. *Nat. Geosci.* **16**, 1151–1158 (2023).
89. De Boeck, P. et al. The estimation of item response models with the lmer function from the lme4 package in R. *J. Stat. Softw.* **39**, 1–28 (2011).
90. Kuznetsova, A., Brockhoff, P. B. & Christensen, R. H. B. lmerTest package: tests in linear mixed effects models. *J. Stat. Softw.* **82**, 1–26 (2017).
91. Nekola, J. C. & White, P. S. The distance decay of similarity in biogeography and ecology. *J. Biogeogr.* **26**, 867–878 (1999).
92. Pohlert, T. Trend: Non-Parametric Trend Tests and Change-Point Detection, R package version 1.1.5, (2023).
93. Ross, G. J. Parametric and nonparametric sequential change detection in R: the cpm Package. *J. Stat. Softw.* **66**, 1–20 (2015).
94. Zhang, Y. L., Li, B. Y. & Zhang, D. A discussion on the boundary and area of the Tibetan Plateau in China. *Geogr. Res.* **21**, 1–8 (2002).

Acknowledgements

We thank the thousands of scientists and researchers who made the field investigation and soil phosphorus measurements in the 1980s. This research was supported by the Second Tibetan Plateau Scientific Expedition and Research Program (2019QZKK0404; X.W.), the National Natural Science Foundation of China (42271070; J.H.), the Technology Major Project of Tibetan Autonomous Region of China (XZ202201ZD0005G01; J.H.), the West Light Scholar of Chinese Academy of Sciences (xbzg-zdsys-202202; J.H.) and the Science and Technology Research Program of Institute of Mountain Hazards and Environment, Chinese Academy of Sciences (IMHE-ZDRW-04; J.H.).

Author contributions

J.H., B.P., and X.W. conceptualized the study and wrote the paper. J.H., B.P., L.Z., S.S., F.L., and Z.D. coded the numerical analyses and analyzed the data based on suggestions from X.W. and P.F. All authors contributed to the discussion and commented on the manuscript.

Competing interests

The authors declare no competing interests.

Additional information

Supplementary information The online version contains supplementary material available at <https://doi.org/10.1038/s41467-025-61501-x>.

Correspondence and requests for materials should be addressed to Xiaodan Wang.

Peer review information *Nature Communications* thanks the anonymous reviewers for their contribution to the peer review of this work. A peer review file is available.

Reprints and permissions information is available at <http://www.nature.com/reprints>

Publisher's note Springer Nature remains neutral with regard to jurisdictional claims in published maps and institutional affiliations.

Open Access This article is licensed under a Creative Commons Attribution-NonCommercial-NoDerivatives 4.0 International License, which permits any non-commercial use, sharing, distribution and reproduction in any medium or format, as long as you give appropriate credit to the original author(s) and the source, provide a link to the Creative Commons licence, and indicate if you modified the licensed material. You do not have permission under this licence to share adapted material derived from this article or parts of it. The images or other third party material in this article are included in the article's Creative Commons licence, unless indicated otherwise in a credit line to the material. If material is not included in the article's Creative Commons licence and your intended use is not permitted by statutory regulation or exceeds the permitted use, you will need to obtain permission directly from the copyright holder. To view a copy of this licence, visit <http://creativecommons.org/licenses/by-nc-nd/4.0/>.

© The Author(s) 2025